JOURNAL OF GEOPHYSICAL RESEARCH, VOL. 113, A09203, doi:10.1029/2008JA013120, 2008

Energetic electron precipitation induced by space based VLF transmitters

P. Kulkarni,[1] U. S. Inan,[1] and T. F. Bell[1]

Received 25 February 2008; revised 20 May 2008; accepted 5 June 2008; published 3 September 2008.

[1] Numerical raytracing with Landau damping is used to calculate electron precipitation that would be induced by in situ sources located at $L = 2$ and $L = 2.5$, at the geomagnetic equator and also at a geomagnetic latitude of 20° along each field line. In accordance with the Wang and Bell (1970) model of antenna radiation in a magnetoplasma, we consider frequencies immediately below, approximately equal to, and 1 kHz above the local lower hybrid resonance frequency at each location and injected rays within 3° of the resonance cone. The magnetospherically reflecting (MR) whistler-mode waves that are injected from such in situ sources propagate with a wave normal angle very close to the resonance cone. Compared to a single-pass interaction, such MR waves precipitate up to 16 times more 100 keV to 5 MeV electrons. Waves injected at initial wave normal angles closer to the magnetic field, e.g., 45°, in fact precipitate fewer >1 MeV electrons than waves injected close to the resonance cone.

Citation: Kulkarni, P., U. S. Inan, and T. F. Bell (2008), Energetic electron precipitation induced by space based VLF transmitters, *J. Geophys. Res.*, *113*, A09203, doi:10.1029/2008JA013120.

1. Introduction

[2] Resonant interactions between energetic electrons and very low-frequency (VLF) waves are an important loss mechanism for trapped particles in the near-Earth space environment [*Kennel and Petschek*, 1966; *Lyons et al.*, 1972; *Inan*, 1987]. A recent study by *Abel and Thorne* [1998a, 1998b] estimated the loss rates of radiation belt electrons in the 100–1500 keV energy range induced by Coulomb collisions and resonant interactions with plasma waves, including plasmaspheric hiss, lightning generated whistlers, and VLF transmitter signals. The authors concluded that man-made VLF transmitters operating continuously in the 17–23 kHz range have a significant impact on 100–1500 keV electron lifetimes.

[3] *Inan et al.* [2003] discussed the feasibility of using an in situ source to inject whistler-mode waves into the inner belts for controlled precipitation of radiation belt electrons. By power scaling the results from *Abel and Thorne* [1998a, 1998b], *Inan et al.* [2003] indicated that a space borne transmitter at operating frequencies of 1–10 kHz can drive diffusion rates that, compared to those from signals from the ground-based VLF transmitters, may be higher by up to a factor of ~30. The high diffusion rates can be further leveraged because whistler-mode waves at the frequencies considered often undergo multiple magnetospheric reflections [*Edgar*, 1972]. A single injected wave packet may endure for several seconds and can be much more efficiently stored in the magnetospheric cavity as compared to the higher wave frequencies from ground-based transmitters that typically make only a single traverse of the magnetosphere. [*Inan et al.*, 2003].

[4] *Kulkarni et al.* [2006] expanded on the results presented in *Inan et al.* [2003] to determine source locations in *L*-shell and geomagnetic latitude, operating frequencies and initial wave normal angles needed to fill the inner radiation belts with whistler-mode wave energy. The authors used the Stanford VLF raytracing code [*Inan and Bell*, 1977], coupled with path-integrated Landau damping and a realistic model [*Wang and Bell*, 1970] of dipole antenna radiation in a magnetoplasma. *Kulkarni et al.* [2006] considered both equatorial and off-equatorial source locations, and concluded that three transmitters radiating in accordance with the *Wang and Bell* [1970] antenna model are sufficient to fill the inner magnetosphere with whistler-mode wave energy, although the authors ignored longitudinal spreading of the rays.

[5] The results of both *Inan et al.* [2003] and *Kulkarni et al.* [2006] lay the groundwork for determining the degree to which in situ injection is a feasible means of achieving controlled precipitation of energetic electrons. The former paper highlighted the effectively larger diffusion brought about by the long lifetimes of low-frequency magnetospherically reflecting (MR) whistler-mode waves. It was noted however that the degree to which such enhanced scattering would come about depends on the efficiency of pitch angle scattering by waves propagating at high angles near the resonance cone. *Kulkarni et al.* [2006] identified specific locations and operating frequencies that would be utilized if such a scheme were to be implemented. However neither study determined the precipitation that would be induced by a space-based source.

[6] In this connection, it is important to note that *Inan et al.* [2003] estimated diffusion based on power scaling the

[1]STAR Laboratory, Stanford University, Stanford, California, USA.

0148-0227/08/2008JA013120$09.00

Table 1. The Wave Frequencies Simulated for the Six Different Injection Sites Considered Here[a]

	Local Lower Hybrid Resonance Frequency			
	$\lambda_s = 0°$		$\lambda_s = 20°$	
	5.4 kHz		9 kHz	−89.3°
L = 1.5	6 kHz	−89.3°	10 kHz	−89°
	7 kHz	−88.9°	11 kHz	−88.8
	2.3 kHz		3.8 kHz	1.24 cm
L = 2.0	2.5 kHz	−89.9°	4.2 kHz	−89.6°
	3.5 kHz	−88.7°	5.2 kHz	−88.9°
	1.2 kHz		2.0 kHz	1.24 cm
L = 2.5	1.3 kHz		2.2 kHz	−89.8°
	2.3 kHz	−88.1°	3.2 kHz	−88.5°

[a]At each location, the middle frequency is approximately equal to the local f_{LHR} while the top and bottom frequencies are ∼10% below and 1 kHz above, respectively. Also shown are the resonance cone angles whenever they exist (i.e. whenever the frequency considered is above the local f_{LHR}). We calculate f_{LHR} using the approximate relation $f_{LHR} \sim (f_{He} f_{Hi})^{1/2}$ where f_{He} is the electron gyrofrequency and f_{Hi} is the ion gyrofrequency.

results from *Abel and Thorne* [1998a, 1998b] and duration of scattering by waves at a constant wave normal angle, ψ, of 45°. Magnetospherically reflecting whistler mode waves, on the other hand, propagate obliquely with ψ near the resonance cone at an angle near 90° (see below). Therefore, the diffusion estimates presented by *Inan et al.* [2003] may not be valid for waves injected from an in situ source at angles near the resonance cone, or after these waves have reflected one or more times (at which time the wave normal angle stays near the resonance cone). If high wave normal angles result in less pitch-angle scattering–a result implied by both *Inan et al.* [2003] and *Inan and Bell* [1991]–the benefit gained by multiple reflections (which enhance the duration of scattering) may be lost. This issue, which was recognized but left unresolved by *Inan et al.* [2003], is addressed here. We use the Stanford VLF Raytracing program [*Inan and Bell*, 1977] to calculate path-integrated Landau damping and determine the precipitation signatures [*Bortnik et al.*, 2006b] that would be induced by an in situ source located in the inner radiation belts.

2. Simulation Procedure

[7] To calculate the energetic (>100 keV) electron precipitation induced by in situ VLF transmitters, we incorporate three separate physical processes: (1) radiation pattern of an antenna immersed in a magnetoplasma, (2) ray paths within the magnetosphere, which depend on magnetic field and particle density models, and (3) resonance interaction between energetic electrons and VLF waves, which induce precipitation based on an assumed electron phase space velocity distribution function and loss-cone pitch angle distribution. For each of these we use theoretical and numerical tools in hand, as described below.

[8] *Wang and Bell* [1970] modeled the radiation properties of a short, electric dipole oriented perpendicular to the ambient magnetic field, radiating in the VLF range, in a magnetoplasma. The authors ignored the effects of the plasma sheath and any warm plasma effects. The *Wang and Bell* [1970] model indicates that a perpendicular dipole in a magnetoplasma emits the bulk of its radiated power as waves at wavelengths approximately equal to the antenna length. For antenna lengths of 200–500 meters and for waves of a few kHz at the source sites considered here, this result effectively restricts the driving frequency, f, to more than ∼90% of the local lower hybrid resonance frequency (f_{LHR}): $f \gtrsim 0.9 f_{LHR}$. Wave frequencies below this cutoff have very long ≳1 km) wavelengths that contain a negligible portion of the radiated energy. In our calculations, the frequency is furthermore limited to 1 kHz above the local f_{LHR} because of strong Landau damping for higher frequencies. Waves operating at frequencies, e.g., 2–3 kHz above the local f_{LHR} are attenuated by more than 10 dB within 1–2 seconds and thus constitute only a small fraction of the total precipitation.

[9] Due of the anisotropic nature of the magnetospheric plasma, the wavelength is strongly dependent on the wave normal, ψ, along with wave frequency. For ψ more than ∼3° from the resonance cone angle, the wavelength is much longer than the antenna length. We therefore consider only k-vectors that lie within 3° of ψ_{res}. See the appendix below for a more complete derivation of this assumption. To summarize, we restrict the frequency from 90% of the local f_{LHR} to 1 kHz above the local f_{LHR}. We also select initial wave normal angles, ψ, to within 3° of the local resonance cone, ψ_{res}. A more detailed description of the rationale with which we limit our choice of the initial wave parameters is given in *Kulkarni et al.* [2006], and the complete derivation can be found in *Wang and Bell* [1969].

[10] In this study, we launch rays representing a wave pulse of a half-second duration from the six locations specified in *Kulkarni et al.* [2006]: L = 1.5, L = 2 and L = 2.5 at the equator and a geomagnetic latitude of 20° for each L-shell. We primarily focus on the last two however because waves injected from L = 1.5 induce significantly less precipitation and often do not even magnetospherically reflect (see below and Figure 6). At each source location, we select three wave frequencies: 90% f_{LHR}, f_{LHR}, and f_{LHR} + 1 kHz. For each frequency, we then launch 30 rays separated by 0.1° in wave normal angle, starting at ψ_{res}. Table 1 shows the source locations, operating frequencies and, if necessary, resonance cone angles considered here. We consider a transmitter with a total radiated power of 1 W and divide this power equally among the rays, assuming that the wave k-vectors are primarily directed along the resonance cone [*Wang and Bell*, 1972]. We then determine the latitudinal and azimuthal (±3°) spread of the rays at 1 km distance (along the ray path) from the source. This calculation results in each ray being assigned an initial Poynting flux of 1×10^{-9} [W/m^2]. However because we are interested in relative comparisons and dependencies of parameters, rather than the absolute amount of induced precipitation, our analyses and conclusions are insensitive to the specific value chosen. Because we use a 2D raytracer, we can only trace rays within the meridional plane and our results thus represent at best a lower limit on the induced precipitation. Including ray paths outside of the meridional plane–as would be possible with a three-dimensional raytracer–may change some of the conclusions presented here. *Cairó and Lefeuvre* [1986] use three-dimensional ray tracing to study the propagation of ELF/VLF hiss in the magnetosphere. Their study indicates that highly oblique whistler waves (with initial wave normal angles in the range

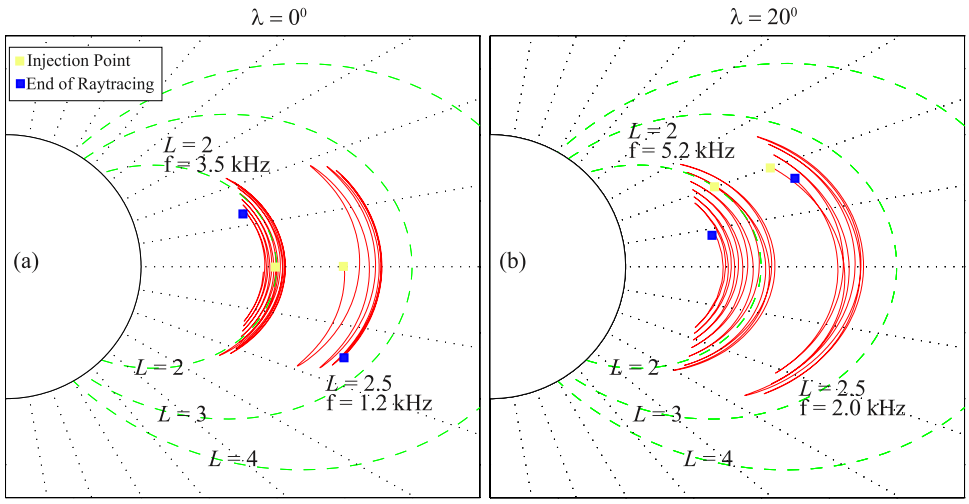

Figure 1. (a) Raypaths calculated by the Stanford VLF Raytracing program for two equatorial injections: 3.5 kHz from L = 2, and 1.2 kHz from L = 2.5. The former is above the local f_{LHR} and propagates inwards, while the latter propagates outward from the source site. (b) Similar to (a), but for injections from $\lambda = 20°$. For the four injections shown, the initial wave normal angle was $-85°$.

considered in this study) tend to stay at an azimuthal angle around $\mathbf{B_o}$, ϕ, which remains approximately constant in the course of their propagation.

[11] The Stanford VLF raytracing program [*Inan and Bell*, 1977] uses a centered dipole model for the magnetic field with an electron gyrofrequency of 880 kHz at the ground at the equator (corresponding to 3.14$e-15$ Tesla). The cold plasma density gradients and the strength and direction of the Earth's magnetic field determine how the rays propagate. We have adopted the *Carpenter and Anderson* [1992] model for the cold plasma density. While the calculated raypaths are density-dependent, adopting the commonly used diffusive equilibrium model of *Angerami and Thomas* [1964] does not significantly change the results. While traversing the magnetosphere, rays also undergo path-integrated Landau damping, which is calculated based on the velocity space distribution function specified in *Bell et al.* [2002].

[12] As the wave energy propagates along the raypath, it interacts with and precipitates energetic electrons. To determine this precipitation, we use the methodology described in *Bortnik et al.* [2006a], which integrates the equations in *Bell* [1984], for different cyclotron resonance modes, m, from $-5 \leq m \leq 5$ to calculate the pitch-angle change induced by in situ sources considered here. To determine the flux of precipitated particles, we apply the calculated pitch-angle change to near loss-cone electrons. This procedure allows us to determine the induced precipitation that would be observed at 100 km altitude at a range of L-shells around the source [*Bortnik et al.*, 2006b].

[13] The AE8 distribution for trapped energetic electrons, with an assumed sinusoidal loss cone pitch-angle distribution, exhibits a sharp dropoff in flux levels with increasing energy [*Vette*, 1991]. While this model would yield more realistic electron precipitation signatures, its use herein obscures our evaluation of the potential efficiency of MR waves at inducing >1 MeV precipitation. The signatures that result from using the AE8 radiation belt model (Figure 4) show large fluxes of <100 keV electrons, and relatively weak fluxes of >1 MeV electrons. However such results preclude us from determining if MR whistler-mode waves are ineffective at scattering >1 MeV electrons, or if weak fluxes occur simply because there too few electrons at those energies to precipitate. We therefore assume a constant flux of 50,000 cm^{-2} s^{-1} $ster^{-1}$ keV^{-1} for all electron energies up to 5 MeV, with a square loss cone pitch-angle distribution. The numerical value is taken to be approximately equal to the 100 keV flux at L = 2 in the AE8 model. Using this somewhat contrived distribution function allows us to make meaningful comparisons between >1 MeV and <1 MeV precipitation.

3. Description of the Wave–Particle Interaction and Electron Precipitation

[14] Before we present our simulation results, it is instructive to first review the relevant physics of MR whistler-mode waves and the wave–particle interaction.

3.1. MR Whistler-Mode Waves

[15] As described above, the low-frequency waves considered here undergo several magnetospheric reflections along their path [*Edgar*, 1976]. Such waves eventually "settle" on an L-shell where the wave frequency is approximately equal to the equatorial f_{LHR}. We simulate frequencies that are close to the local f_{LHR} at each source location and inject these waves at initial wave normal angles very close to ψ_{res}, which implies that the injected waves do not travel far from the source site. In both *Kulkarni et al.* [2006] and the results shown below, the region of illumination is $\sim\pm 0.1L$ of the source L-shell. While the slowest variation of ω_H occurs around the equator and thus equatorial scattering often dominates the precipitation signature (see below and *Inan et al.* [1982]), off-equatorial wave–particle interactions can also be important. See Figure 1 for raypaths of several in situ injections. In each panel, the left (right)

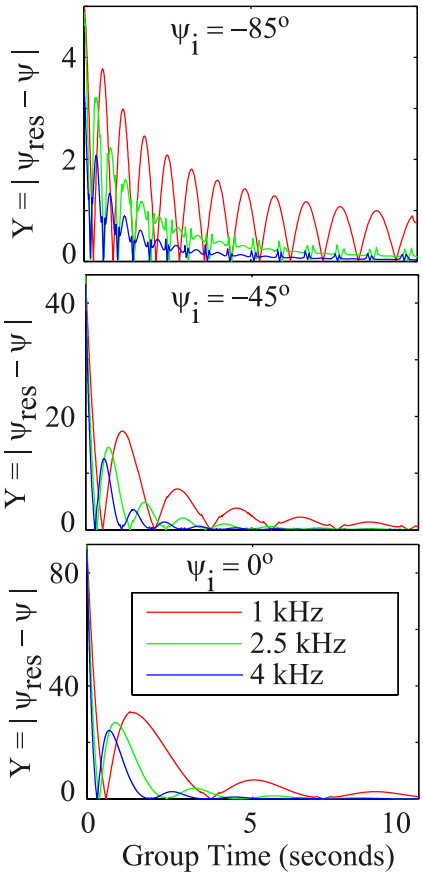

Figure 2. (a)–(c) $Y = |\psi - \psi_{res}|$ for three different wave frequencies and initial wave normal angles, all injected from the equator at $L = 2$. The quasi-periodicity seen is a result of repeated magnetospheric reflections along the raypath. Note that regardless of frequency or initial wave normal angle, ψ rapidly ends up very close to the resonance cone.

injection is above (below) the local f_{LHR}. Note that f_{LHR} increases off the equator, and thus 5.2 kHz waves injected from $\lambda = 20°$ move inward because the equatorial f_{LHR} at $L = 2$ is ~2.5 kHz.

[16] To understand the precipitation signatures shown below, additional features of MR whistler-mode propagation need to be elucidated. First, wave frequencies below the equatorial f_{LHR} on the source L-shell tend to propagate away from the Earth and persist for several tens of seconds, while frequencies above the equatorial f_{LHR} tend to propagate toward the Earth and are Landau damped very quickly [*Kulkarni et al.*, 2006; *Bortnik et al.*, 2003]. Off-equatorial injections result in stronger Landau damping than equatorial ones because such waves are above the local f_{LHR} for a longer time along their path. For wave frequencies above the local f_{LHR}, the refractive index surface, $\mu(\psi)$, is open and the refractive index can have a large magnitude, which leads to strong damping [*Bortnik et al.*, 2003]. Our simulation results show that off-equatorial interactions induce shorter-lived precipitation signatures. However, despite the shorter lifetimes, the higher-resonant energies off the equator result in higher >1 MeV precipitation fluxes (see below).

[17] Another important point is that MR whistler-mode waves generally propagate with wave normal angles very close to ψ_{res} [*Jasna et al.*, 1990]. One way to view the results is to examine the variation of the quantity $Y = \psi - \psi_{res}$, where ψ is the wave normal angle along the raypath, as is done in Figure 4 of *Jasna et al.* [1990]. Figure 2 shows Y along a raypath for waves injected from $L = 2$ at the equator, for wave frequencies of 1, 2.5 and 4 kHz, and initial wave normal angles of $\psi = -85°$, $-45°$, and $0°$. Note that regardless of operating frequency, initial wave normal angle, or whether the frequency is below or above the local f_{LHR}, the wave normal angle ψ approaches the resonance cone ($Y \sim 1°$) within 10 seconds. Wave frequencies just below or above the local f_{LHR}, ~2.5 kHz, approach the resonance cone even more quickly.

[18] This last point is relevant from the point of view of the feasibility of using in situ injection to precipitate energetic electrons. *Kulkarni et al.* [2006] suggested that the restricted initial wave normal angles implied by the *Wang and Bell* [1970] model limited the region of illumination. While this statement is true, a more important factor may be the scattering efficiency. Even if it were possible to effectively radiate at low wave normal angles of, e.g., 45°, the propagation characteristics in a cold, smooth magnetoplasma would remain the same. Within two to three magnetospheric reflections, all waves attain wave normal angles very close to the resonance cone regardless of wave frequency or initial ψ. Thus in the cold, smooth magnetoplasma considered here, all MR whistler-mode waves attain have wave normal angles close to the resonance cone. These resultant high wave normal angles might negatively impact scattering efficiency as was suggested by *Inan et al.* [2003].

3.2. Wave-Particle Interaction

[19] *Bell* [1984] gives the gyro-averaged equations of motion for the resonance interaction between an obliquely propagating whistler-mode wave and an energetic electron for a general harmonic resonance m:

$$\frac{d\alpha}{dt} = -\frac{\omega_{\tau m}^2}{k_z v_\perp}\left(1 + \frac{\omega \cos^2\alpha}{m\omega_H - \omega}\right)\sin\eta + \frac{v_\perp}{2\gamma\omega_H}\frac{\partial\omega_H}{\partial z} \qquad (1)$$

where $\omega_{\tau m}^2 = (-1)^{m-1}\omega_{\tau 0}^2[J_{m-1}(\beta) - \alpha_1 J_{m+1}(\beta) + \gamma\alpha_2 J_m(\beta)]$, $\omega_{\tau 0}^2 = (\omega_1 k_z p_\perp/\gamma m_e)$, $\omega_1 = (e/2m_e)(B_x^w + B_y^w)$, ω_2 $\omega_2 = (e/2m_e)(B_x^w - B_y^w)$, $\alpha_1 = (\omega_2/\omega_1)$, $\alpha_2 = (eE_z^w/\omega_1 p_\perp)$, $\beta = (k_x p_\perp/m_e\gamma\omega_H)$, $\gamma = 1/\sqrt{(}(1 - v^2/c^2)$, $k_z = k\cos\psi = (\omega\mu/c)$ $\cos\psi$, $k_x = k\sin\psi$, where k is the wave k-vector, μ is the refractive index, J_i are Bessel functions of the first kind of order i, $v_\perp$ is the component of the electron velocity perpendicular to the ambient magnetic field, ψ is measured with respect to the ambient magnetic field assumed to be in the z-direction, B_x^w, B_y^w, E_z^w are the magnetic and electric field components of the whistler-mode wave, η is the phase between the right hand component of the wave magnetic field and $v_\perp$, and ω_H is the electron gyrofrequency.

[20] Equation (1) shows that the electron pitch-angle changes as a result of both wave forces and adiabatic variation. In principle, an electron would be trapped indefinitely on a given field line in the absence of wave forces [*Walt*, 1994, p. 42]. The wave forces can induce a change in the electron equatorial pitch angle which otherwise remains constant during adiabatic motion. Wave-induced pitch-angle change accumulates only when the phase angle η remains constant for extended periods. This restriction implies that

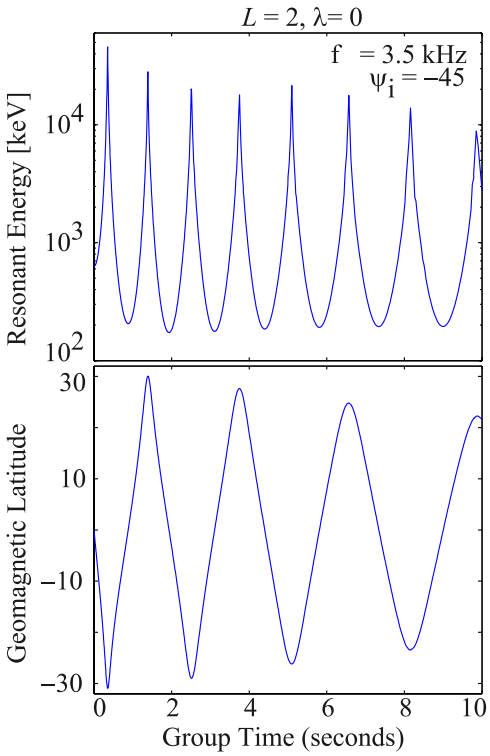

Figure 3. The top shows resonant electron energy along the raypath for the m = 1 resonance mode for a 3.5-kHz wave injected from the equator at L = 2. The bottom shows geomagnetic latitude along raypath. Note that E_{res} increases off the equator, and that the resonant energy stays above 100 keV at all points along the raypath.

$d\eta/dt$ = 0, which leads to the resonance condition between an energetic electron and a whistler-mode wave:

$$v_z = \frac{m\omega_H/\gamma - \omega}{k_z} = \frac{m\omega_H/\gamma - \omega}{\omega\mu\cos\psi}c \qquad (2)$$

where v_z is the resonant electron velocity along the Earth's magnetic field, m, an integer, is the resonant mode, and the remaining terms have been defined above [*Bell*, 1984].

[21] We now highlight relevant features of the above two equations, starting with equation (2). This equation shows how location (which affects ω_H and k_z) and ω affect resonant velocity: v_z is inversely proportional to ω and directly proportional to ω_H if k_z is constant. Moreover, as the absolute value of m increases, the resonant energy increases. Non-zero m indicates transverse or cyclotron resonance between the wave magnetic field and electron, while m = 0 represents the Landau resonance. Figure 3 shows plots of resonant electron energy, for m = 1, along raypath. Note that resonant energy, E_{res}, increases off the equator because ω_H increases away from the equator (a similar plot was also shown in *Jasna et al.* [1990]). The low wave frequencies of 1–5 kHz injected from an in situ source always undergo cyclotron resonance with electrons of energies >100 keV, and often resonate with >1 MeV electrons. Note that as ψ increases, $k_z = \omega\mu\cos\psi/c$ decreases if everything else is constant. Smaller k_z in turn leads to higher parallel resonant energies as shown in equation 2. Thus a wave propagating at, e.g., ψ = 45°, generally resonates with lower energy electrons than a wave propagating at ψ = 85°. These high resonant electron energies, along with long lifetimes due to magnetospheric reflections, are among the reasons that led *Inan et al.* [2003] to suggest in situ injection could be a promising means of achieving controlled precipitation of MeV electrons.

[22] As a MR whistler-mode propagates, it resonates with and pitch-angle scatters energetic electrons at all points along its path. However the inhomogeneity of the Earth's magnetic field plays a dominant role in determining the wave–particle interaction time (or the duration of the resonant scattering). Slower variation of magnetic field amplitude, which occurs at the equator, allows the resonant wave–particle interaction to endure for a longer time (per particle) and thus often leads to the strongest precipitation [*Inan et al.*, 1982]. Also note that several terms in equation (1) depends on the wave normal angle, ψ, between the wave k-vector and $\mathbf{B}_0$. The wave normal angle can thus play a crucial role in determining the precipitation signatures induced by an in situ source. *Inan et al.* [2003] noted that high wave normal angles are associated with decreased pitch-angle scattering, which might inhibit the effectiveness of an in situ source.

[23] To summarize: MR whistler-mode waves undergo cyclotron resonance with >100 keV and >1 MeV electrons along their path. Pitch-angle scattering however is most effective near the magnetic equator and partially depends on the wave-normal angle ψ. The k-vector of an MR whistler-mode wave stays very close to ψ_{res} during most if its raypath (regardless of the initial value emitted by the source), which results in large electron resonant velocities and which also affects pitch-angle scattering efficiency.

[24] We should also note that in our simulations we specifically calculate precipitation induced by a one-half second long VLF pulse. Future in situ sources however operate continuously, and thus may have long-term effect on the pitch-angle distribution of energetic electrons that are not revealed in our calculations. Nevertheless, a recent study by *Shprits et al.* [2006] documented that electron lifetimes are primarily governed by the value of pitch angle scattering close to the loss cone. Accordingly, it is likely that the induced precipitation of loss-cone energetic electrons as is calculated here may indeed yield useful information regarding the long-term effects of in situ VLF sources. However this study only examines the effect of a short pulse on a very small range of pitch angles near the loss cone, which will not directly affect the entire distribution. If we were considering continuous precipitation then we would have to examine the complete pitch angle distribution and work toward a solution based on diffusion concepts. This issue should be examined in greater detail in future studies.

[25] We now return to the primary question raised in *Inan et al.* [2003] regarding the effectiveness of in situ injection to achieve controlled precipitation: do the benefits of high v_z and long lifetimes due to magnetospheric reflections outweigh the possible reduced pitch-angle scattering associated with wave normal angles close to ψ_{res}? We must highlight that in their study, *Inan et al.* [2003] calculated diffusion coefficients versus wave frequency and resonance harmonic number for 1.5 MeV and 3 MeV electrons at a single

Table 2. The Number of Precipitated Electrons and Cavity Gain Factors for the Source Locations and Frequencies Considered Here[a]

		Number of Precipitated Electrons		Cavity Gain Factor	
		>100 keV	>1 MeV	>100 keV	>1 MeV
	5.4 kHz	0.039	0.038	211.2	216.3
$L = 1.5$, $\lambda = 0°$	6 kHz	0.026	0.024	23.5	22.4
	7 kHz	0.073	0.072	36.7	36.2
	9 kHz	0.033	0.033	1	1
$L = 1.5$, $\lambda = 20°$	10 kHz	0.043	0.043	1	1
	11 kHz	0.052	0.052	1	1
	2.3 kHz	1.57	1.57	16.1	16.1
$L = 2$, $\lambda = 0°$	2.5 kHz	1.89	1.89	15.9	15.9
	3.5 kHz	2.20	2.18	10.5	10.5
	3.8 kHz	4.37	4.24	14.5	14.1
$L = 2$, $\lambda = 20°$	4.2 kHz	3.47	3.32	10.7	10.2
	5.2 kHz	2.33	2.10	5.6	5.4
	1.2 kHz	8.96	8.91	10.8	10.7
$L = 2.5$, $\lambda = 0°$	1.3 kHz	8.61	8.52	9.4	9.4
	2.3 kHz	5.65	4.29	4.2	5.3
	2.0 kHz	16.76	13.98	6.9	6.3
$L = 2.5$, $\lambda = 20°$	2.2 kHz	14.56	11.65	6.1	5.8
	3.2 kHz	6.93	4.85	2.8	3.1

[a]9 kHz, 10 kHz, and 11 kHz waves injected from $L = 1.5$ do not magnetospherically reflect and the cavity gain factor is exactly 1.

equatorial location. Resonant wave frequency versus ψ was also shown at only that source location. *Albert* [1999], another study that implies large ψ leads to weak diffusion, keeps ψ constant and calculates resonant frequencies. Such is not the case however for the precipitation induced by an in situ source: the wave frequency is fixed, but ψ changes along the raypath and the wave undergoes both cyclotron and Landau resonance, at different points in space, with electrons from ~10 keV to >1 MeV.

[26] Because plasma and wave parameters, such as ω_H and μ, vary along the raypath, we should not infer the total >1 MeV precipitation induced by MR whistler-mode waves from the diffusion of 1.5 MeV electrons calculated at a single location. In fact, as our simulation results show, waves injected at ψ close to ψ_{res} can induce more >1 MeV precipitation than waves injected parallel to $\mathbf{B}_0$.

4. Simulation Results and Analysis

[27] We first briefly address sources located at $L = 1.5$, and then proceed with analyzing the results from sources at $L = 2$ and $L = 2.5$. We focus on the latter two source locations because waves injected from those locations induce significantly more precipitation than sources at $L = 1.5$. Table 2 and Figure 6 show that waves injected from that location precipitate approximately 100 times fewer 100 keV - 5 MeV electrons than the corresponding frequencies at the remaining locations. (Figure 6 should be compared with the results shown in Figures 7 and 8). Moreover, the 9 kHz, 10 kHz and 11 kHz waves that would be injected from a source at $L = 1.5$, $\lambda = 20°$ do not magnetospherically reflect and therefore the cavity gain factor is exactly 1. (The total number of precipitated electrons equals the number precipitated before the first reflection). Our calculations do reveal that an equatorial source at $L = 1.5$ does produce relatively large cavity gain factors. This benefit however is offset by weak precipitation. The primary reason for relatively little induced precipitation is the extremely high electron resonant energies, from 3 MeV up to ~27 MeV, at locations close to the Earth's surface (see analysis and equation 2 above). If it ever becomes necessary to precipitate >5 MeV electrons very close to the Earth's surface (L ~1.5), then 5.4 kHz, 6 kHz, and 7 kHz waves from the equator at $L = 1.5$ should be particularly effective. Except for a short analysis on magnetospheric hiss waves in the last paragraph, the remainder of this section focuses on sources at $L = 2$ and $L = 2.5$.

[28] Figure 4 displays differential number flux at 100 km altitude induced by an equatorial source at $L = 2$. We show the energy-time signatures of precipitation that would be observed in the northern and southern hemispheres at 100 km altitude at a range of L−shells around that of the source. These results show the combined effect of including resonance modes $-5 \leq m \leq 5$, and both equatorial and off-equatorial interactions. In this figure alone, we use the AE8 radiation belt for the trapped radiation fluxes. In other words, the precipitation flux values are representative of those that would be measured in practice for a total radiated wave power of 1 Watt.

[29] The f_{LHR} at $L = 2$ at the equator is ~2.5 kHz. Note, first, that 2.3 kHz waves propagate outward to $L \sim 2.1$, and persist for more than 20 seconds. The precipitation signature induced by 3.5 kHz waves, on the other hand, moves inward to $L = 1.9$ and the waves induce precipitation for a much shorter period of time. The quasi-periodicity seen in all the panels is a result of the interaction occurring primarily near the equator. Because the waves magnetospherically reflect, we observe precipitation bursts roughly with the predicity governed by the time it takes for the wave to reach the equator. Second, note that there are large, intense precipitation peaks <100 keV, and very weak, sometimes barely visible, precipitation bursts ≳1 Mev. The former peaks are the result of the Landau resonance, and the latter case is due largely to cyclotron resonance. Because these two interactions represent different physical mechanisms, certain electron energies often do not resonate with a given wave. Furthermore, there are many more electrons at lower energies and thus the differential number flux will be more intense.

[30] For the rest of this study, we use the constant initial electron distribution function as described above. Our goal is to quantify the amount of additional >100 keV and >1 MeV precipitation that occurs as a result of the MR process. To that end, we calculate the number of energetic electrons precipitated before and after the first magnetospheric reflection. To be consistent with *Inan et al.* [2003], we denote this parameter the cavity gain factor. In this study however the gain represents additional precipitation, not solely the number of equatorial crossings weighted by wave power density. We then compare the cavity gain factor for all the wave frequencies and source locations considered here.

[31] Figure 5 shows the differential number flux, in the northern hemisphere, precipitated by a 3.5 kHz equatorial source at $L = 2$. For these calculations, we use a constant distribution function of 50,000 cm^{-2} s^{-1} $ster^{-1}$ keV^{-1} with a square loss-cone. Thus the results greatly underestimate (overestimate) the actual <100 (>100) keV electron precipitation (see Figure 4 for a more realistic precipitation signature). Compared to Figure 4, the >1 MeV precipitation in Figure 5 is much stronger relative to the <1 MeV

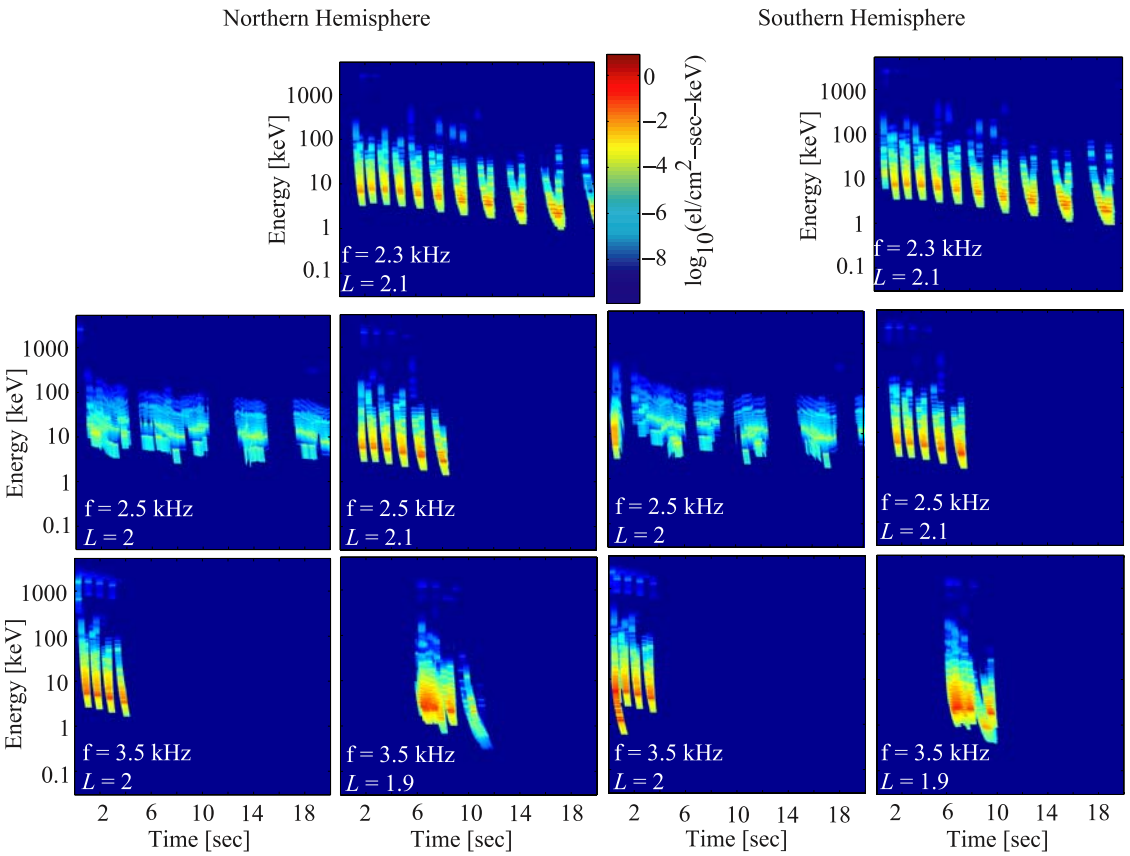

Figure 4. Differential number flux at 100 km altitude induced by an equatorial source at $L = 2$. The left (right) two columns display the flux induced at the northern (southern) hemisphere. Shown across the rows are three different operating frequencies: 2.3 kHz, 2.5 kHz and 3.5 kHz (from top to bottom). Individual parts show where, in L-shell, precipitation occurs. Note that 3.5 kHz–above the local f_{LHR} of 2.5 kHz–moves inwards, while 2.3 kHz moves outwards.

precipitation. In fact, during the first 3–4 reflections, precipitation for electrons both above and below 1 MeV is approximately equal. As the wave settles at $L = 1.9$ after several reflections, the precipitation flux for >1 MeV electrons is 2–3 orders of magnitude weaker than for <1 MeV electrons. In Figure 4, the >1 MeV precipitation is approximately 8 orders of magnitude lower at all times. Those apparently substantially weaker signatures therefore result largely from the AE8 distribution, which contains relatively few energetic electrons, rather than the presumed inefficient scattering induced by MR whistler-mode waves. Figure 5 shows that MR whistler-mode waves propagating at high wave normal angles can effectively precipitate >1 MeV electrons. Moreover, MR whistler-mode waves resonate with much higher-energy electrons because large ψ increases resonant electron velocity through smaller k_z (see discussion above). Even if ψ extremely close $\lesssim 0.5°$) to ψ_{res}, which occurs after the first few reflections, leads to decreased scattering efficiency, the much larger resonant electron energies appear to compensate, so that >1 MeV precipitation fluxes are not lower (Figure 6).

[32] Table 2 shows the "cavity gain factors" for >100 keV and >1 MeV for all the source locations and frequencies considered here. We include the total number of precipitated electrons in both the northern and southern hemisphere. We should reiterate that these numerical results

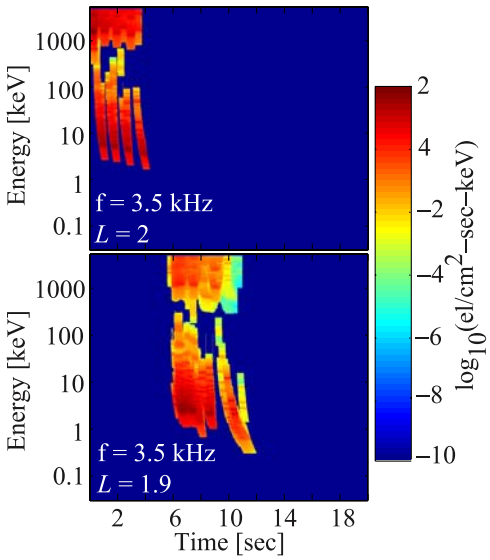

Figure 5. Differential number flux in the northern hemisphere at $L = 2$ and $L = 1.9$ induced by a 3.5 kHz equatorial source at $L = 2$. These results used a constant energetic electron distribution function of 50,000 cm^{-2} s^{-1} $ster^{-1}$ keV^{-1} with a square loss-cone. Note that, compared to Figure 4, the >1 MeV precipitation is relatively strong.

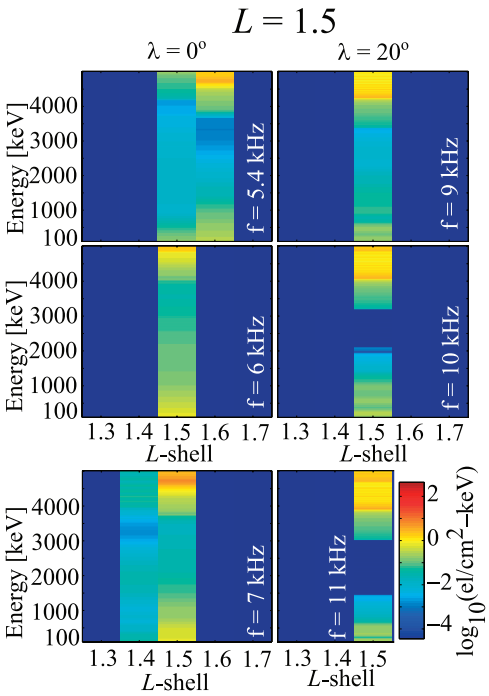

Figure 6. Precipitation and illumination spectra induced by sources at L = 1.5, at the geomagnetic equator and a latitude of 20°. Note that, compared to Figure 7 and Figure 8, there is much less precipitation induced by sources at L = 1.5.

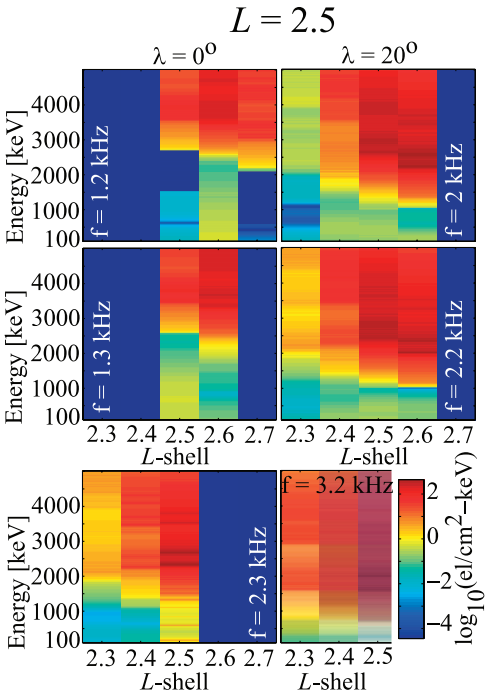

Figure 8. Similar to Figure 6, except for sources at L = 2.5. Although the region of illumination is at higher L-shells, the general trends are similar and explained in the text.

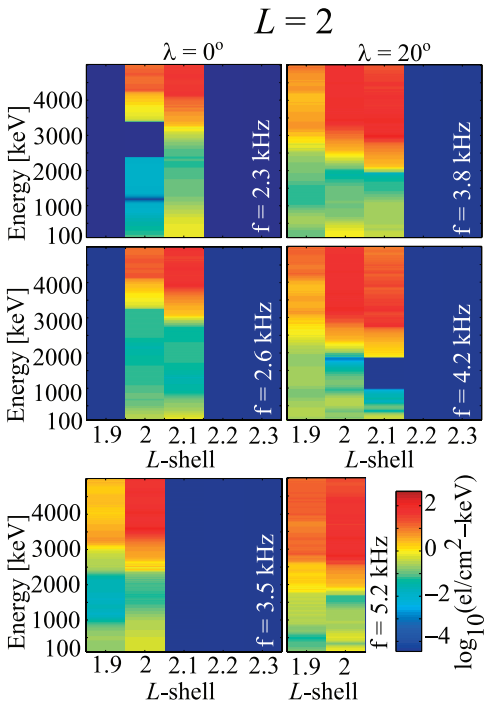

Figure 7. Precipitation and illumination spectra induced by sources at L = 2 at the geomagnetic equator and a latitude of 20°. These results were obtained by integrating the differential number flux (Figures 4 and 5) over time. Note that off-equatorial injections induce stronger signatures.

are based on a constant energetic electron distribution function. The relevant trends can be explained as follows: For each source, except for an equatorial source at L = 2, higher wave frequencies induce less precipitation because of shorter lifetimes. At the equator at L = 2 however 2.3 kHz and 2.5 kHz waves undergo cyclotron resonance primarily with >5 MeV. Thus the total induced precipitation is relatively low because our initial energetic electron distribution contains no electrons >5 MeV in energy. For all source locations, the cavity gain factor decreases with frequency due to, once again, shorter lifetimes, which leads to fewer magnetospheric reflections. For 3.5 kHz waves, e.g., there is relatively less precipitation induced after the first pass than for 2.5 kHz waves. Off-equatorial sources induce stronger precipitation because resonance energy increases at higher latitudes, and the longer raypaths therefore resonate with more energetic electrons. The decreased scattering efficiency at higher latitudes [*Inan et al.*, 1982] appears to be less important than high resonant energy. Finally, the stronger precipitation fluxes for a source located at L = 2.5, compared to L = 2, occur because waves injected from that source location have longer lifetimes (not shown). In all cases, magnetospheric reflections precipitate several times more >1 MeV electrons as compared to a single pass interaction. These results demonstrate that the MR whistler mode waves that are injected from in situ sources may be effective at controlled precipitation of energetic electrons, and more so specifically because of their multiple reflections in the magnetospheric cavity.

[33] Figure 7 and 8 show the precipitation and illumination spectra for the source sites and frequencies just discussed. Note that waves with frequencies below (above) the

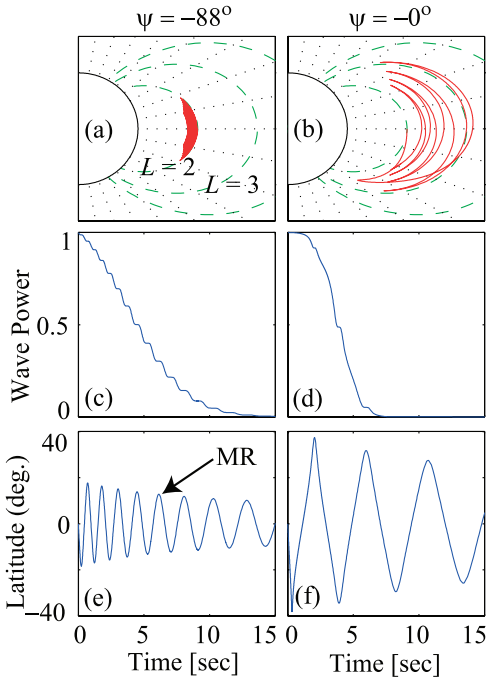

Figure 9. Raypaths, Landau damping and latitude along raypath for two 3.5 kHz rays injected from $L = 2$. The left column displays these parameters for a ray with an initial wave normal angle of $-88°$, while the right column is for $\psi = 0°$.

local equatorial f_{LHR} precipitate electrons primarily at L-shells higher (lower) than the source location. Also note that off-equatorial sources induce stronger >1 MeV precipitation signatures, and that higher frequencies generally induce weaker ones. The exception for an equatorial source at $L = 2$ was explained above. In this case, Figure 7 shows that 2.3 kHz and 2.5 kHz waves only precipitate 3–5 MeV electrons, while 3.5 kHz waves resonate with electron energies down to 2 MeV.

[34] The results shown thus far are all based on sources radiating waves close to the local f_{LHR} and injected at initial wave normal angles very close to the resonance cone. Such waves tend to remain close to the source site and settle very quickly at an L-shell. Furthermore, such waves tend to persist for 15 to 20 seconds before being Landau damped by as much as 10 dB. Waves injected with less oblique wave normal angles, on the other hand, propagate much farther from the source and have relatively short lifetimes [*Kulkarni et al.*, 2006]. Although we have restricted the initial wave normal angle, it is still be instructive to compare the precipitation induced by waves with lower initial ψ with our previous calculations. These results would be useful in the event that a longer antenna can be used to effectively radiate at initial ψ far from the resonance cone.

[35] Figure 9a and 9b shows two 3.5 kHz rays injected, at initial ψ of $-88°$ (Ray 1) and $-45°$ (Ray 2), from the geomagnetic equator at $L = 2$. The middle panel shows the Landau damping along the raypath for these two rays. There are several relevant features that we must highlight. Note that Ray 1 stays very close to the source L-shell, persists for ~15 seconds, and magnetospherically reflects several (actually 17) times very close to the geomagnetic equator. In fact, the ray stays within ±10° of the equatorial region. Ray 2, on the other hand, propagates up to $L \sim 3$, is Landau damped by 10 dB within 10 seconds, magnetospherically reflects only 7 times, and propagates up to a geomagnetic latitude of ~30°. Shorter lifetimes and fewer magnetospheric reflections imply that waves injected at lower initial ψ precipitate fewer energetic electrons as compared to the results shown earlier. Moreover, waves injected at low initial ψ (e.g., Ray 2) propagate up to relatively high geomagnetic latitudes along the field line where pitch-angle scattering is relatively inefficient because of the more rapid gradients of the Earth's magnetic field [*Inan et al.*, 1982].

[36] Table 3 compares the >100 keV and >1 MeV electron precipitation induced by a 3.5 kHz equatorial source at $L = 2$. We follow an identical procedure as described above, but consider 30 rays centered at 0°, −25°, −45° and −65° instead of near the resonance cone. For reference, the last row reproduces the results shown in Table 2, where the rays were injected within 3° of ψ_{res}. Note that waves injected at less oblique initial wave normal angles generally precipitate fewer >1 MeV electrons. The >100 keV precipitation however is stronger when the initial wave normal angle is closer to $\mathbf{B}_0$ because the larger k_z leads to lower resonant energies than waves with ψ close to ψ_{res}. Although such waves are less effective at inducing >1 MeV electron precipitation, they do precipitate electrons at a broader range of L-shells. Figure 10 shows the precipitation and illumination spectra for the range of initial wave normal angles just described. Note that the precipitation is generally stronger at lower energies, and that increasing ψ leads to illumination over a narrower range of L-shells. For waves injected at $\psi \sim 0°$, the ray paths are such that certain L-shells are not illuminated with whistler-mode wave energy (see Figure 9b).

[37] Our results indicate that that MR whistler-mode waves injected at high initial wave normal angles from an in situ source may be more effective than previously thought at inducing >1 MeV electron precipitation [*Inan et al.*, 2003]. Compared to a single-pass interaction, multiple reflections sometimes induce more than an order of magnitude more energetic electron precipitation. However only locations within ~0.1 L of the source site can be effectively targeted with such in situ injection. Projecting whistler-mode wave energy to more distant L-shells require injecting high power waves at low ≲45°) initial wave normal angles, typically not feasible at electrical dipole antenna lengths of a few hundred meters. Even if such injection were possible, such waves are Landau damped relatively quickly and induce less >1 MeV precipitation. These two conclusions together imply that illuminating a broad region of the magnetosphere may

Table 3. The Number of Precipitated Electrons and Cavity Gain Factors for Different Initial Wave Normal Angles for a 3.5-kHz Equatorial Source at $L = 2$

	Number of Precipitated Electrons		Cavity Gain Factor	
	>100 keV	>1 MeV	>100 keV	>1 MeV
0°	2.38	1.09	14.6	21.7
25°	3.90	1.32	32.4	80.7
45°	1.83	0.73	18.3	51.0
65°	2.94	2.06	21.4	51.4
~87°	2.20	2.18	10.5	10.5

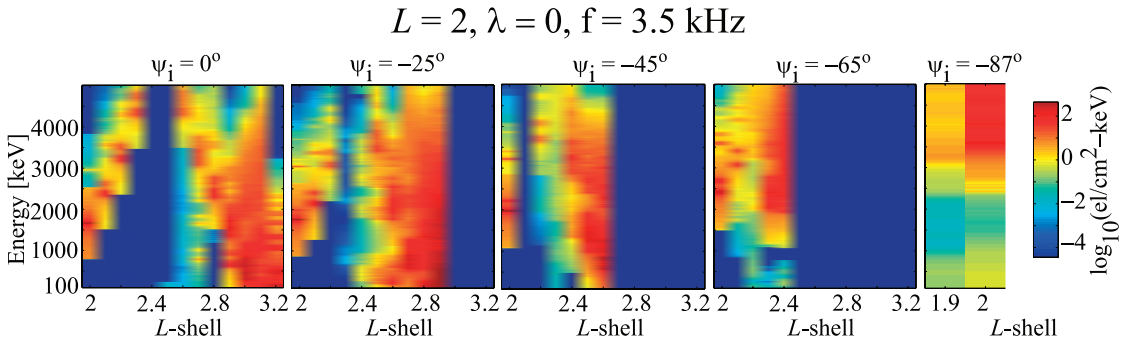

Figure 10. Precipitation and illumination spectra for 3.5 kHz waves injected at a range of initial wave normal angles. In all parts, the source site was at the equator at $L = 2$. Note that lower initial ψ spreads wave power over a broader range of L-shells, but the precipitation signature is generally weaker at higher energies.

require several sources distributed radially. Further investigation is required to determine if three-dimensional raytracing, warm plasma effects, or the existence of density irregularities would change this conclusion.

[38] As a final note, we briefly consider natural processes, and especially magnetospheric hiss waves, that induce electron precipitation at $L = 2$ to $L = 2.5$. Previous studies [*Lyons et al.*, 1972; *Meredith et al.*, 2007] have suggested that magnetospheric hiss plays an important role depleting energetic electrons from those L-shells. The landmark study by *Abel and Thorne* [1998a, 1998b] however concluded that man-made VLF transmitters are needed to account for the observed electron lifetimes below $L \lesssim 2.6$. Anthropogenic sources—including possible future in situ transmitters—thus may be important in any future scheme of controlled precipitation at these L-shells. An in situ source at $L = 1.5$ might also be an important driver of precipitation at low L-shells, despite the weak precipitation signatures shown here.

5. Summary and Conclusions

[39] We have calculated precipitation signatures for four different in situ sources located at $L = 1.5$, $L = 2.0$, 2.5, at the geomagnetic equator and a latitude of 20°. We incorporated the *Wang and Bell* [1970] model for a short, electric dipole immersed in a magnetoplasma to restrict both the operating frequency and initial wave normal angle of the injected rays. For each source location, we thus selected three operating frequencies around the local lower hybrid resonance frequency, f_{LHR}: 0.9 f_{LHR}, $\sim f_{LHR}$, and f_{LHR} + 1 kHz. For each wave frequency, we launched 30 rays from the resonance cone, ψ_{res}, to ψ_{res} + 3°. We used the Stanford VLF raytracing program [*Inan and Bell*, 1977] to calculate raypaths based on a simple dipole model for the Earth's magnetic field and the *Carpenter and Anderson* [1992] model for the particle density. We incorporated the effects of Landau damping along the raypath, and used the velocity space distribution function specified in *Bell et al.* [2002]. The results of the raytracing and Landau damping calculation were then used to determine the induced energetic electron precipitation based on the methodology described in *Bortnik et al.* [2006a].

[40] In a cold, smooth magnetoplasma, magnetospherically reflecting (MR) whistler-mode waves, after a few reflections, propagate at wave normal angles very close to ψ_{res}. This outcome is relatively insensitive to operating frequency or initial ψ. As they propagate, MR whistler-mode waves undergo both Landau and cyclotron resonance with electrons in the Earth's radiation belts. The Landau resonant particles are <100 keV, and mostly <10 keV. Cyclotron resonance occurs with >100 keV electrons, and resonant energies can be as high a few MeV. The wave–particle interaction is most effective near the geomagnetic equator because the slow variation of the Earth's magnetic field allows for the longest interaction time.

[41] We have defined the cavity gain factor, a ratio of total electrons precipitated to the number precipitated before the first reflection. Calculating the cavity gain factor for the different source location and operating frequency configurations show that, compared to a single-pass interaction, MR whistler-mode waves induce substantial >100 keV and >1 MeV electron precipitation. Equatorial sources radiating just below or at the local f_{LHR} induce the most >1 MeV precipitation, and off-equatorial sources induce the least. These results indicate that an in situ source radiating waves close to the local f_{LHR} at high initial wave normal angles may be effective at inducing controlled precipitation of energetic electrons. We also determined the precipitation that would be induced by sources radiating waves at much lower initial ψ. Waves injected at lower initial wave normal angles are damped more quickly, undergo fewer magnetospheric reflections, and propagate up to high latitudes where pitch-angle scattering is relatively inefficient [*Inan et al.*, 1982]. A source that could radiate at low initial ψ would therefore be less effective than one that injects waves at ψ close to ψ_{res}.

[42] Future studies should determine the effect of including three-dimensional raytracing, a warm plasma analysis, and magnetic-field density irregularities. The work of *Hashimoto et al.* [1977], for example, indicates that the effects of the resonance cone may be moderated if we include a non-zero particle temperature, and might modify the results shown here.

Appendix A: Justification for Initial Wave-Normal Angle Restriction

[43] The antenna factor described in *Wang and Bell* [1969] and *Kulkarni et al.* [2006] is given as:

$$F(k) = \frac{\sin^4 kl}{(kl)^4} \tag{A1}$$

[44] As shown in (B4) of Appendix B of *Wang and Bell* [1969], the leading term of the radiation resistance for a dipole antenna in a magnetoplasma oriented along the x axis perpendicular to the ambient magnetic field is:

$$R_{\perp} \simeq 2\ln(2/b\beta)\mathrm{A_o}\int_0^{\infty}\frac{\sin^4(\lambda p)}{(\lambda p)^4}\,p^2dp \qquad \text{(A2)}$$

where b is the antenna radius, $p = n_x$, the refractive index along the x axis, and $\lambda p = \mathrm{h}k_x/2$, where h is the antenna half length, and where:

$$\mathrm{A_o} = \mathrm{Z_o}(h\beta/2\pi)^2/\sqrt{|\epsilon_s\epsilon_o|} \qquad \text{(A3)}$$

[45] If we now take the factor $(h\beta/2)^2$ from A_o and bring it into the integral, the integral can be written:

$$R_{\perp} \simeq \mathrm{B_o}\int_0^{\infty}\frac{\sin^4 q}{q^2}\,dp \qquad \text{(A4)}$$

where $\mathrm{B_o} = 2\ln(2/b\beta)\mathrm{Z_o}/(\pi^2\sqrt{|\epsilon_s\epsilon_o|})$ and $q = \lambda p$.

[46] It can be shown that the integrand in (A4) has maxima when $\tan q = 2q$. The dominant maximum occurs for $q = 1.17$, or equivalently, for $\lambda p \simeq 1$. Therefore the major part of the radiation resistance is contributed by waves for which $\lambda n_x \simeq 1$. To be more specific, if we let the -3 dB points define the range over which the integrand of (A4) is significant, then we find the important values of λp to be:

$$0.6 \le \lambda p \le 1.8 \qquad \text{(A5)}$$

[47] **Acknowledgments.** This research was supported by the Department of the Air Force under grant F19628-03-C-0059-P000003.

[48] Zuyin Pu thanks Yuri Shprits and Jay Albert for their assistance in evaluating this paper.

References

Abel, B., and R. M. Thorne (1998a), Electron scattering loss in the Earth's inner magnetosphere: 1. Dominant physical processes, *J. Geophys. Res.*, *103*, 2385. (Correction, *J. Geophys. Res.*, *104*, 4627 (1999))

Abel, B., and R. M. Thorne (1998b), Electron scattering loss in the Earth's inner magnetosphere: 2. Sensitivity to model parameters, *J. Geophys. Res.*, *103*, 2397. (Correction, *J. Geophys. Res.*, *104*, 4627 (1999))

Albert, J. M. (1999), Analysis of quasi-linear diffusion coefficients, *J. Geophys. Res.*, *104*, 2429.

Angerami, J. J., and J. O. Thomas (1964), Studies of planetary atmospheres, 1, The distribution of electrons and ions in the Earth's exosphere, *J. Geophys. Res.*, *69*, 4537.

Bell, T. F. (1984), The nonlinear gyroresonance interaction between energetic electrons and coherent VLF waves propagating at an arbitrary angle with respect to the Earth's magnetic-field, *J. Geophys. Res.*, *89*(A2), 905–918.

Bell, T. F., U. S. Inan, J. Bortnik, and J. D. Scudder (2002), The Landau damping of magnetospherically reflected whistlers within the plasmasphere, *Geophys. Res. Lett.*, *29*(15), 1733, doi:10.1029/2002GL014752.

Bortnik, J., U. S. Inan, and T. F. Bell (2003), Energy distribution and lifetime of magnetospherically reflecting whistlers in the plasmasphere, *J. Geophys. Res.*, *108*(A5), 1199, doi:10.1029/2002JA009316.

Bortnik, J., U. S. Inan, and T. F. Bell (2006a), Temporal signatures of radiation belt electron precipitation induced by lightning generated MR whistler waves. Part I: Methodology, *J. Geophys. Res.*, *111*, A02204, doi:10.1029/2005JA011182.

Bortnik, J., U. S. Inan, and T. F. Bell (2006b), Temporal signatures of radiation belt electron precipitation induced by lightning generated MR whistler waves. Part II: Global signatures, *J. Geophys. Res.*, *111*, A02205, doi:10.1029/2005JA011398.

Cairó, L., and F. Lefeuvre (1986), Localization of sources of ELF/VLF hiss observed in the magnetosphere: Three-dimensional ray tracing, *J. Geophys. Res.*, *91*, 4352.

Carpenter, D. L., and R. R. Anderson (1992), An ISEE/Whistler model of equatorial electron-density in the magnetosphere, *J. Geophys. Res.*, *97*(A2), 1097–1108.

Edgar, B. C. (1972), The structure of the magnetosphere as deduced from magnetospherically reflected whistlers, *Tech. Rep. 3438-2*, Radiosc. Lab., Stanford Electron. Lab., Stanford Univ., Stanford, Cali.

Edgar, B. C. (1976), The upper and lower frequency cutoffs of magnetospherically reflected whistlers, *J. Geophys. Res.*, *81*, 205.

Hashimoto, K., I. Kimura, and H. Kumagai (1977), Estimation of electron temperature by VLF waves propagating in directions near the resonance cone, *Planet Space Sci*, *25*, 871.

Inan, U. S. (1987), Gyroresonant pitch angle scattering by coherent and incoherent whistler mode waves in the magnetosphere, *J. Geophys. Res.*, *92*, 127.

Inan, U. S., and T. F. Bell (1977), The plasmapause as a VLF waveguide, *J. Geophys. Res.*, *82*, 2819.

Inan, U. S., and T. F. Bell (1991), Pitch angle scattering of energetic particles by oblique whistler waves, *Geophys. Res. Lett.*, *18*(1), 49–52.

Inan, U. S., T. F. Bell, and H. C. Chang (1982), Particle-precipitation induced by short-duration VLF waves in the magnetosphere, *J. Geophys. Res.*, *87*(A8), 6243–6264.

Inan, U. S., T. F. Bell, J. Bortnik, and J. M. Albert (2003), Controlled precipitation of radiation belt electrons, *J. Geophys. Res.*, *108*(A5), 1186, doi:10.1029/2002JA009580.

Jasna, D., U. S. Inan, and T. F. Bell (1990), Equatorial gyroresonance between electrons and magnetospherically reflected whistlers, *Geophys. Res. Lett.*, *17*(11), 1865–1868.

Kennel, C. F., and H. E. Petschek (1966), Limit on stably trapped particle fluxes, *J. Geophys. Res.*, *99*(1).

Kulkarni, P., U. S. Inan, and T. F. Bell (2006), Whistler mode illumination of the plasmaspheric resonant cavity via in situ injection of ELF/VLF waves, *J. Geophys. Res.*, *111*, A10215, doi:10.1029/2006JA011654.

Lyons, L. R., R. M. Thorne, and C. F. Kennel (1972), Pitch angle diffusion of radiation belt electrons within the plasmasphere, *J. Geophys. Res.*, *77*, 3455.

Meredith, N. P., R. B. Horne, S. A. Glauert, and R. R. Anderson (2007), Slot region electron loss timescales due to plasmaspheric hiss and lightning-generated whistlers, *J. Geophys. Res.*, *112*, A08214, doi:10.1029/2007JA012413.

Shprits, Y. Y., W. Li, and R. M. Thorne (2006), Controlling effect of the pitch angle scattering rates near the edge of the loss cone on electron lifetimes, *J. Geophys. Res.*, *111*, A12206, doi:10.1029/2006JA011758.

Vette, J. (1991), The AE-8 trapped electron model environment, *National Space Science Data Center*, Report 91–24, Greenbelt, Maryland.

Walt, M. (1994), *Introduction to Geomagnetically Trapped Radiation*, Cambridge Univ. Press.

Wang, T. N. C., and T. F. Bell (1969), Radiation resistance of a short dipole immersed in a cold magnetoionic medium, *Radio Sci*, *4*(2), 167–177.

Wang, T. N. C., and T. F. Bell (1970), On the VLF/ELF radiation resistance of an electric dipole in a cold magnetoplasma, *Radio Sci*, *5*(3), 605.

Wang, T. N. C., and T. F. Bell (1972), VLF/ELF radiation patterns of arbitrarily oriented electric and magnetic dipoles in a cold lossless multicomponent magnetoplasma, *J. Geophys. Res.*, *77*(7), 1174–1189.

T. F. Bell, U. S. Inan, and P. Kulkarni, STAR Laboratory, Stanford University, 301 Packard Bldg., MC 9515, 350 Serra Mall, Stanford, CA 94305, USA. (pxk161@stanford.edu)